Thermochimica Acta 513 (2011) 33–37

Contents lists available at ScienceDirect

Thermochimica Acta

journal homepage: www.elsevier.com/locate/tca

An in-depth *in situ* IR study of the thermal decomposition of barium trifluoroacetate hydrate

M. Mosiadz[a,*], K.L. Juda[a,b], S.C. Hopkins[a], J. Soloducho[b], B.A. Glowacki[a,c]

[a] Department of Materials Science and Metallurgy, University of Cambridge, Pembroke Street, Cambridge CB2 3QZ, United Kingdom
[b] Department of Chemistry, Wroclaw University of Technology, Wybrzeze Wyspianskiego 27, 50-370 Wroclaw, Poland
[c] Institute of Power Engineering, ul.Augustowka 6, 02-981 Warsaw, Poland

ARTICLE INFO

Article history:
Received 10 September 2010
Received in revised form 12 October 2010
Accepted 2 November 2010
Available online 11 November 2010

Keywords:
Barium trifluoroacetate
Difluoromethylene diradical
Barium fluoride
HR-TG
FT-IR
DSC

ABSTRACT

The pyrolysis of $Ba(CF_3COO)_2{\cdot}nH_2O$ at temperatures up to 1000 °C, under flowing pure Ar, O_2 and O_2 saturated with water vapour, was extensively analysed. The existence of a:CF_2 diradical is inferred and the formation of HF is observed directly for the first time during a trifluoroacetic acid salt decomposition. High resolution thermogravimetry, differential scanning calorimetry, X-ray diffractometry and scanning electron microscopy indicated that the exothermic two-stage decomposition of the anhydrate salt occurs between 282 and 325 °C, forming BaF_2 via an unstable $CF_3COOBaF$ intermediate. Fourier transform infrared spectroscopy revealed the influence of water on the reactions of the liberated gaseous products, identifying CF_3COOH, HF, CHF_3 and CO_2 as the principal volatile species, with C_2F_4, C_2F_6, CO and SiF_4 also detected. The decomposition temperature is significantly lower than previously reported, which has implications for sol–gel processing.

1. Introduction

Fluoride glasses are used in optical and opto-electronic applications [1–3], as immiscible transparent matrices for functional fine particles [4,5] or as host crystals for luminescent ions [6]. In such glasses, a low concentration of transition metal ions results in strong absorptions in the infrared range of the spectrum, which are unacceptable in many applications [7,8]. Metal fluorides are not commonly available in the required ultra-high purity, so metal trifluoroacetates are commonly used as affordable, high purity starting materials. The same trifluoroacetate salts are the most popular metal cation precursors in the synthesis of superconducting $YBa_2Cu_3O_{7-\delta}$ coated conductors (YBCO CC), as they inhibit the formation of carbon-rich impurities, for example $BaCO_3$, during post-deposition heat treatment [9].

Barium trifluoroacetate has been successfully used in anti-refracting coatings [10,11] and YBCO CC thin film deposition [12–14] via a sol–gel method (chemical solution deposition, CSD). Unlike evaporation techniques, which often require ultra-high vacuum (physical vapour deposition, PVD), the sol–gel approach is cheap and can be easily scaled up; but controlling the crucial transformation of the deposited gel into a film with the right morphology is challenging. A thorough analysis and understanding of the decomposition process can contribute to controlling this transformation and optimising the material's final performance.

It is assumed that the formation of metal fluorides results from the thermal decomposition of the trifluoroacetic acid anions coordinated to the metal cations. In the present work we present the results of an in-depth *in situ* IR study of the thermal decomposition of barium trifluoroacetate hydrate, as a full understanding of pyrolysis is of great importance during any sol–gel deposition technique.

2. Experimental

2.1. Chemicals

Barium(II) trifluoroacetate hydrate (Ba-TFA, $Ba(CF_3COOH)_2{\cdot}nH_2O$) was obtained from Alfa Aesar (JM) and used as supplied.

2.2. Characterisation techniques

Thermogravimetry (TG) and high resolution thermogravimetry (HR-TG) coupled with Fourier transform infrared (FT-IR) spectroscopy were performed using a TA Instruments TGA Q500 in an open platinum crucible. For standard TG, a heating rate of 5 °C/min was used from room temperature to 1000 °C. HR-TG was performed up to 600 °C, with a heating rate dynamically adjusted in response

* Corresponding author. Tel.: +44 (0) 1223 767933; fax: +44 (0) 1223 334567.
E-mail address: mm701@cam.ac.uk (M. Mosiadz).

0040-6031/$ – see front matter © 2010 Elsevier B.V. All rights reserved.
doi:10.1016/j.tca.2010.11.004

to the measured rate of change of mass in the range from 0 to 20 °C/min. Analysed samples were between 5 and 10 mg in mass. The mixture of evolved and purge gases was transferred to the heated stainless steel gas cell of a Thermo Scientific Nicolet iS10 Spectrometer via inert glass-lined stainless steel tubing, which was also heated to around 125 °C to avoid the condensation of less volatile species. Spectra were recorded at appropriate intervals throughout each run. All data collected from TG and HR-TG were analysed in TA Universal Analysis software, and differentiated to obtain differential thermogravimetry (DTG) data. The start of a reaction was defined from the mass vs. temperature curve by the intersection of the extrapolated local horizontal baseline and the tangent to the curve at its steepest point [15]. The equipment was purged before each measurement for 0.5 h at ambient temperature before a background IR spectrum was taken.

Simultaneous thermogravimetry and differential scanning calorimetry (TG–DSC) were performed using a TA Instruments SDT Q600 in an open platinum crucible with a heating rate of 5 °C/min from room temperature to 1000 °C. Analysed samples were between 5 and 10 mg in mass each. Data were analysed in TA Universal Analysis software, with the same definition of the start of a reaction as used for TG. Results are presented here using the convention of a positive peak in the temperature difference between the sample and the reference for an exothermic process and a negative trough for an endothermic process.

The TG, HR-TG and TG–DSC measurements were all performed in three different atmospheres with a flow rate of 100 mL/min: pure Ar, O_2, and O_2 saturated with water vapour. The water-saturated atmosphere was prepared at standard temperature and pressure (25 °C, 1 atm). Every experiment was repeated 3 times in order to confirm the results and gain enough powder for X-ray diffractometry.

X-ray diffractometry (XRD) was performed on powder samples using Philips X'Pert PW1730 diffractometers. The instruments used the Bragg–Brentano geometry and unfiltered Cu Kα radiation. $\theta/2\theta$ scans were performed with 1/2° divergence and anti-scatter slits and a 0.3 mm receiving slit to minimize variations in measured intensity as a result of the finite sample area (typically 1 cm^2). All powder diffraction data were analysed in Panalytical Highscore Plus software and compared with the International Centre for Diffraction Data (ICDD) powder diffraction file PDF2.

Scanning electron microscopy (SEM) was performed on powder samples using a JEOL JSM 5800 LV scanning microscope with a W source and an ultra-thin window (UTW) detector for energy dispersive X-ray (EDX) spectroscopy. The detector was calibrated each time against Si. All SEM images and EDX data were analysed in INCA software.

3. Results

The results of thermogravimetric analysis revealed two distinct regions of mass loss, the first below 150 °C associated with three peaks in DTG, and the second larger mass loss starting at 286 °C and corresponding to two poorly resolved peaks in DTG (Fig. 1). In order to resolve these partially overlapping peaks and to identify the evolved gases of decomposition, the compound was subjected to HR-TG coupled with FT-IR in three different purge gases, dry Ar, pure O_2 and O_2 saturated with water vapour. It was confirmed by FT-IR analysis that the mass loss at low temperatures, up to 150 °C, corresponded to water loss. Fig. 2 shows the HR-TG curves in all three atmospheres for this dehydration region: three broad steps are observed in each case, but they are much more clearly defined for the wet O_2 atmosphere. The mass loss after the third dehydration step is consistent with the starting material existing as a dihydrate (Tables 1 and 2): from HR-TG data in all three atmospheres, $n = 1.9 \pm 0.1$.

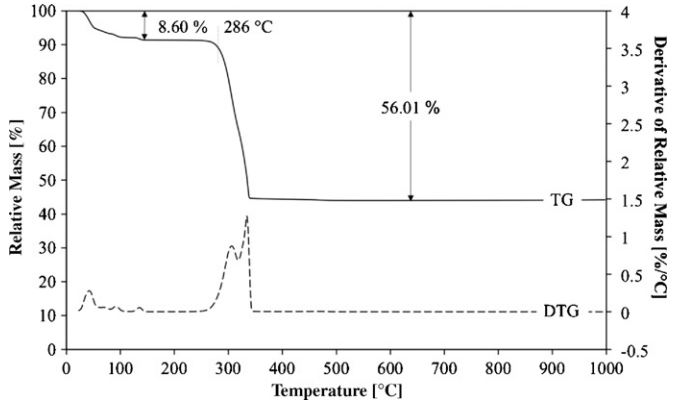

Fig. 1. TG and DTG curves of Ba-TFA hydrate heated at 5 °C/min under a flowing dry Ar atmosphere, revealing overlapping decomposition steps of the salt; above 150 °C, the same behaviour was observed in all three atmospheres.

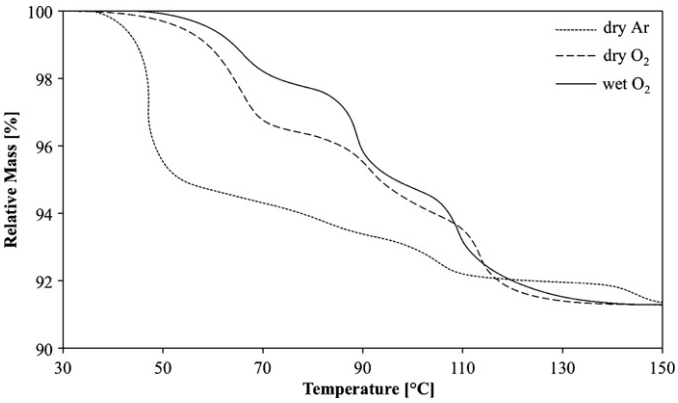

Fig. 2. Dehydration HR-TG curves of Ba-TFA hydrate heated under three different flowing atmospheres, revealing the presence of two intermediate hydrates.

Fig. 3 shows the full temperature range of the HR-TG data. After a broad plateau above 150 °C, during which no mass loss occurred, the rapid decomposition of the anhydrate salt at 292 °C resulted in a sharp mass loss with a changing gradient, reaching a horizontal plateau at 325 °C. The corresponding DTG curve has two peaks in this temperature range, revealing a two-stage decomposition mechanism: the start temperature for the first stage, and the remaining masses after each stage, are listed in Table 2. In all the atmospheres used here, the remaining masses after the first and second stages are in good agreement with those expected for $CF_3COOBaF$ and BaF_2 respectively. After this decomposition, no

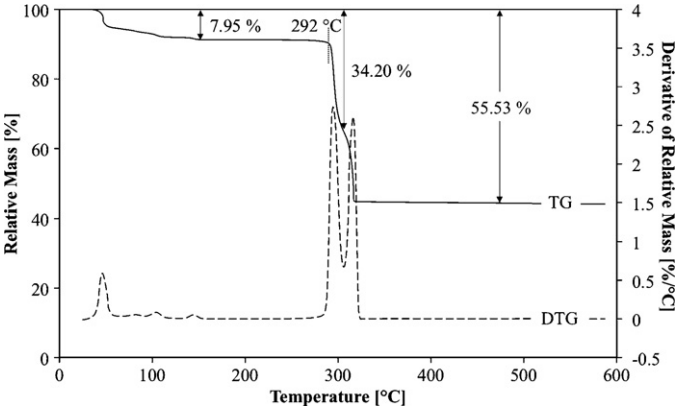

Fig. 3. HR-TG and DTG curves of Ba-TFA hydrate heated under a flowing dry Ar atmosphere with resolved decomposition peaks of the anhydrous salt; above 150 °C, identical curves were recorded under a flowing dry and wet O_2 atmosphere.

Table 1
TG data for Ba-TFA Hydrate decomposition under 5 °C/min heating rate, showing the relative remaining mass after dehydration and decomposition. The theoretical values are calculated on the assumption that the starting material is a dihydrate, $n = 2$.

Compound	Flowing atmosphere	Mass % as anhydrous $Ba(CF_3COO)_2$		Decomposition temperature (°C)	Mass % as BaF_2	
		Theory	Found		Theory	Found
$Ba(CF_3COO)_2 \cdot nH_2O$	Dry Ar	90.98	91.40	286	43.90	43.99
	Dry O_2	90.98	92.37	286	43.90	44.45

Table 2
HR-TG data for Ba-TFA hydrate decomposition, showing the relative remaining mass after dehydration and the two stages of decomposition. The theoretical values are calculated on the assumption that the starting material is a dihydrate, $n = 2$.

Compound	Flowing atmosphere	Mass % as anhydrous $Ba(CF_3COO)_2$		Decomposition temperature (°C)	Mass % as $CF_3COOBaF$ (1st stage)		Mass % as BaF_2 (2nd stage)	
		Theory	Found		Theory	Found	Theory	Found
$Ba(CF_3COO)_2 \cdot nH_2O$	Dry Ar	90.98	92.05	292 ± 2	67.44	65.80	43.90	44.47
	Dry O_2	90.98	91.56	288 ± 1	67.44	69.56	43.90	44.34
	Wet O_2	90.98	91.02	282 ± 1	67.44	67.00	43.90	43.86

further mass changes were observed up to the maximum temperatures of 600 °C and 1000 °C reached in HR-TG and TG respectively.

In order to confirm the products remaining after decomposition, samples were collected for XRD. Fig. 4 shows the diffraction pattern of the white powder remaining after HR-TG was performed up to a temperature of 600 °C, demonstrating that this product was BaF_2. EDX analysis of the same powder indicated the Ba/F atomic ratio to be 1.9 ± 0.2 (Fig. 5). The product after performing TG up to 1000 °C was also a white powder confirmed by XRD to be phase-pure BaF_2.

FT-IR analysis of evolved gases identified a mixture of carbon dioxide (CO_2) and monoxide (CO) as well as a mixture of fluorinated compounds. The evolution of CO_2 and CO is represented by the carbonyl stretch at 3726, 3700, 3627, 2362, 2337, 667 cm^{-1}, and peaks at 2178 and 2111 cm^{-1}, respectively. The fluorinated mixture principally consisted of trifluoroacetic acid (TFAH), trifluoromethane (CHF_3) and hexafluoroethane (C_2F_6), with traces of tetrafluoroethene (C_2F_4). The principal changes in the spectrum with temperature are the appearance and loss of TFAH peaks at 3579, 1829, 1405, 1234, 1203, 1120, 778 and 580 cm^{-1} as well as CHF_3 peaks at 3035, 1375 and 1151 cm^{-1}, associated with the carbonyl (C=O), C–H, C–C and C–F stretches listed in Table 3. Peaks corresponding to C_2F_6 were also observed at 1250, 1115 and 714 cm^{-1} in the early stages of decomposition. The formation of C_2F_4 is observed from the peaks at 1338 and 1186 cm^{-1}, and the peaks at 3920, 3877, 3833 and 3788 cm^{-1} are evidence of the presence of hydrogen fluoride (HF) in the gas mixture. A peak at 1026 cm^{-1} develops for silicon tetrafluoride (SiF_4), which is believed to be a reaction product between HF and either the quartz elements of the furnace tube or the glass spectroscopic cell [16,25]. Repeated analysis did not reveal any carbonyl fluoride (COF_2) to be present. A list of all recognised species is presented in Table 3 together with the assigned stretching regions and references.

The rate of evolution of each detected species, as reflected by the absorbance in the FT-IR data (Fig. 7), depended on temperature and atmosphere. For the dry atmospheres, significant amounts of CO_2 and TFAH with a smaller amount of C_2F_6 were detected throughout decomposition; significant amounts of SiF_4 and CHF_3 were liberated only during the second stage of decomposition, above ~310 °C. In the case of the O_2 atmosphere saturated with water vapour, only CO_2 was evolved rapidly in both stages of decomposition: the other four species, although detected in the first step, exceeded 50% of their maximum absorbances during the second stage of the decomposition.

Analysis of the TG–DSC curves (Fig. 6) revealed the presence of three endothermic peaks in the temperature range in which dehydration takes place, followed by two exothermic peaks. Accurate temperature calculation was difficult because the DSC baseline was not straight. The endotherms (a, b and c) are due to dehydration, and the first (d) and second (e) exotherm correspond to the two-

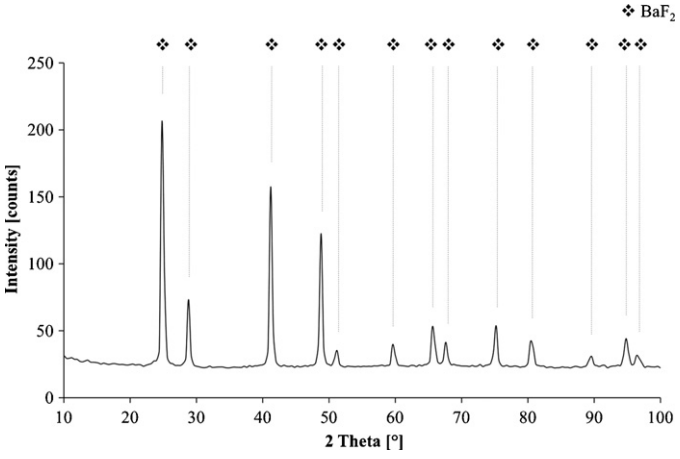

Fig. 4. XRD 2θ scan (Cu Kα) of the residue after heating Ba-TFA Hydrate to 600 °C under a flowing dry Ar atmosphere during HR-TG, revealing BaF_2 formation; identical patterns were recorded for the powder samples obtain under a flowing dry and wet O_2 atmosphere.

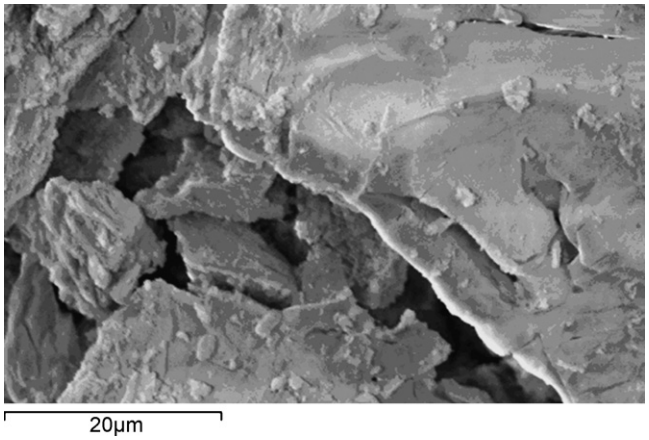

Fig. 5. SEM micrograph (secondary electron image) of the Ba-TFA hydrate residue after HR-TG under a flowing dry Ar atmosphere; EDX analysis suggested a F/Ba ratio of 1.9 ± 0.2.

Table 3
Assignment of IR peaks (4000–400 cm^{-1}) recorded during HR-TG of Ba-TFA hydrate under a flowing dry Ar atmosphere.

Observed peak (cm^{-1})	Species	Approximate description	Reference
3920	HF	H–F	[16,17]
3877	HF	H–F	[16,17]
3833	HF	H–F	[16,17]
3788	HF	H–F	[16,17]
3726	CO_2	C=O	[18]
3700	CO_2	C=O	[18]
3627	CO_2	C=O	[18]
3579	CF_3COOH	O–H str	[16,18–20]
3035	CHF_3	C–H str	[16,18]
2362	CO_2	C=O asym str	[16,18]
2337	CO_2	C=O asym str	[16,18]
2178	CO	C≡O	[16,18]
2111	CO	C≡O	[16,18]
1829	CF_3COOH	C=O str	[16,18–20]
1405	CF_3COOH	C–O str	[16,18–20]
1375	CHF_3	C–F str	[16,18]
1338	C_2F_4	C–F str	[18,21]
1250	C_2F_6	C–F str	[18]
1234	CF_3COOH	C–F asym str	[16,18–20]
1203	CF_3COOH	C–F sym str C–C str	[16,18–20]
1186	C_2F_4	C–F oop def	[18,21]
1151	CHF_3	C–F str	[16,18]
1120	CF_3COOH	O–H ip def	[16,18–20]
1115	C_2F_6	C–F str	[18]
1026	SiF_4	Si–F str	[22–24]
778	CF_3COOH	C–C ip def	[16,18–20]
720	C_2F_6	C–C str	[18]
701	CHF_3	C–F def	[16,18]
667	CO_2 CF_3COOH	C=O def	[18–20]
580	CF_3COOH	C–F ip sym def	[16,18–20]

str, stretching; def, deformation; sym, symmetric; asym, asymmetric; ip, in-plane; oop, out-of-plane.

stage decomposition of the anhydrous compound. These results are in agreement with TG and HR-TG, where three dehydration steps of the dihydrate and then two decomposition steps of the anhydrous salt were defined.

4. Discussion

The low temperature of the dehydration reaction indicates that the water molecules are not strongly bonded to the salt (Reaction (1)). HR-TG confirmed that dehydration proceeded in three steps, forming intermediate hydrates with masses and stability ranges dependent on the atmosphere. Although it is believed that the salt's crystalline structure could change upon dehydration, as occurs in the TFA salts of lanthanides [25], the intermediates were not stable enough to isolate for further characterisation.

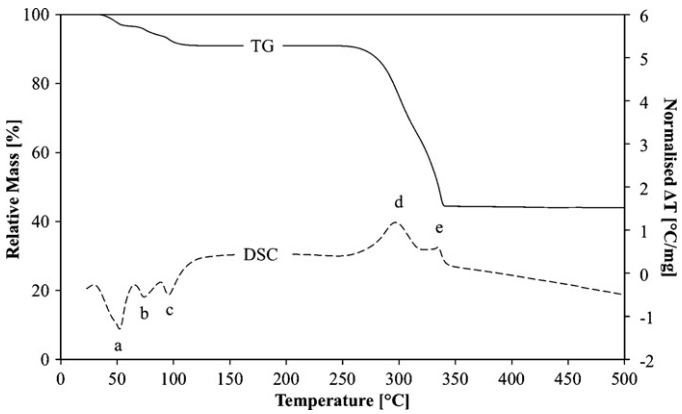

Fig. 6. TG and DSC (exothermic positive) curves of Ba-TFA Hydrate heated at 5 °C/min under a flowing wet O_2 atmosphere, revealing the three-stage endothermic dehydration (a, b and c) of the hydrate and the exothermic two-stage decomposition of the anhydrous salt (d and e); identical curves were recorded under a flowing dry O_2 atmosphere.

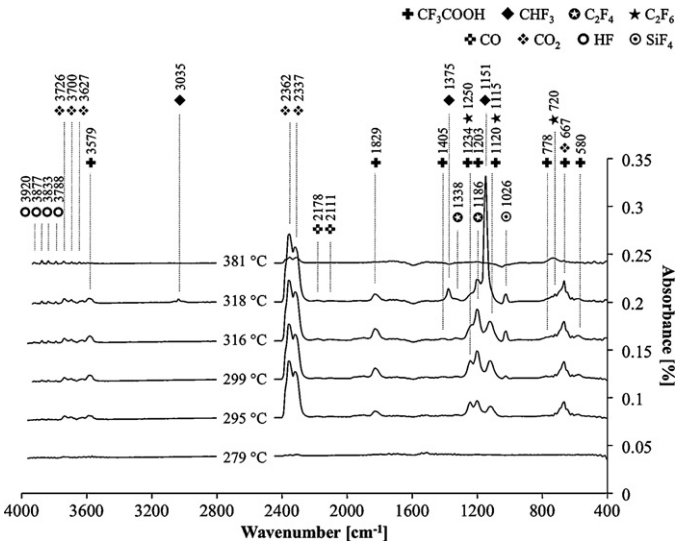

Fig. 7. FT-IR spectrum of gases evolved during HR-TG of Ba-TFA hydrate under a flowing dry Ar atmosphere, revealing liberation of HF, CO_2, CF_3COOH, CHF_3, CO, C_2F_4, C_2F_6 and SiF_4 at the indicated temperatures (curves offset for clarity).

Thermal studies revealed the decomposition of anhydrous Ba-TFA to start at a temperature around 290 °C in the presence of flowing dry gases and almost 10 °C lower in the presence of flowing wet gases (Table 2). From the HR-TG and DSC curves it can be seen that the two partially overlapping stages of decomposition are highly exothermic and that the intermediate species is unstable, as it undergoes further decomposition readily before the first has been completed. Although powder XRD analysis could not be carried out after the first exothermic decomposition step, the mass change is consistent with the formation of $CF_3COOBaF$. Calculations of the remaining mass together with XRD powder analysis confirmed the final product of decomposition to be BaF_2.

The existence of a:CF_2CO_2 diradical has been postulated (but not conclusively demonstrated) in earlier work on the thermal decomposition [26,27] and flash photolysis [28] of TFAH and related species. However, in the present work, the volatile products detected together with calculations of remaining mass suggest that the decomposition of anhydrous Ba-TFA proceeds stepwise through the liberation of CO_2 and a difluoromethylene diradical (:CF_2), not a:CF_2CO_2 diradical (Reaction (2)). The existence of:CF_2 has previously been suggested in several related systems, including the TFAH scavenging reaction with Br_2 [23] and THAH pyrolysis in the presence of flowing Br_2 [24]; in each case, CF_2Br_2 was identified in the IR spectrum. Furthermore, pyrolysis of a TFAH and HCl mixture has been shown (by IR) to produce $CHClF_2$ [12], and trimethyltrifluoromethyltin ($(CH_3)_3SnCF_3$) has been reported to produce:CF_2 on decomposition [29].

The liberation of:CF_2 from unstable $CF_3COOBaF$ is also believed to take place in the second stage of decomposition, leaving BaF_2 as the final product (Reaction (3)). The formation of traces of C_2F_4 in the present study, presumably from the dimerisation of:CF_2, is further verification of the presence of:CF_2 in the reaction mixture (Reaction (4)). The:CF_2 may also react in contact with quartz or glass components, giving the SiF_4 observed by FT-IR (Reaction (5)) [16].

TFAH and HF are both observed in the FT-IR spectra during the decomposition of anhydrous Ba-TFA, even in the supposedly dry atmospheres. In the absence of any other proton source, it must be proposed that water is still present in the system (either in the gas cell of the IR spectrometer or at low concentrations in the purge gas), and that HF is formed from its reaction with:CF_2 (Reaction (6))

[16]. The HF may then, most likely in the presence of:CF_2 and CO_2, produce TFAH (Reaction (7)).:CF_2 seems to react relatively easily with H_2O, since little C_2F_4 and no higher polymer was formed.

The majority of HF seems to react either with:CF_2 to form a significant amount of CHF_3 (Reaction (8)) [16], or with the quartz elements of the furnace tube or the glass spectroscopic cell to form SiF_4 (Reaction (9)) [16,26]. The former reaction is not unexpected given the previously reported reactivity of:CF_2 with HCl [12].

$$(CF_3COO)_2Ba{\cdot}2H_2O = (CF_3COO)_2Ba + 2H_2O \quad (1)$$

$$(CF_3COO)_2Ba = CF_3COOBaF + :CF_2 + CO_2 \quad (2)$$

$$CF_3COOBaF = BaF_2 + :CF_2 + CO_2 \quad (3)$$

$$2{:}CF_2 = C_2F_4 \quad (4)$$

$$2{:}CF_2 + SiO_2 = SiF_4 + 2CO \quad (5)$$

$$:CF_2 + H_2O = 2HF + CO \quad (6)$$

$$:CF_2 + HF + CO_2 = CF_3COOH \quad (7)$$

$$HF + :CF_2 = CHF_3 \quad (8)$$

$$4HF + SiO_2 = SiF_4 + 2H_2O \quad (9)$$

No evidence of BaO was found, suggesting that the hydrolysis of BaF_2 has to take place at a temperature above 1000 °C in the conditions investigated here. Tada et al. [30] reported oxide formation starting at 800 °C in sol–gel thin films, but a lower reaction temperature is not uncommon for thin film deposition by sol–gel routes [32].

In the complete absence of water, it is expected that Reactions (6)–(9) would not occur, and the decomposition described by Reactions (2) and (3) would be consistent with the overall reaction proposed by Rüssel for Li, Na, Mg, Al, Ca, Ti, Zn, Y, Zr, Ba, La and Pb TFA salts (Reaction (10); M = metal cation) [10]. However, the present work has distinguished a two-stage mechanism and demonstrated the role of:CF_2.

$$(CF_3COO)_xM = MF_x + (1/2)xC_2F_4 + xCO_2 \quad (10)$$

The onset temperatures found in this work for the decomposition of anhydrous Ba-TFA, 282 °C in wet O_2 and 288–292 °C in dry atmospheres, are significantly lower than the 318 °C and 346 ± 2 °C previously reported by Tada et al. [30] and Rüssel [10] respectively. In sol–gel processing routes, too high a heating rate around the decomposition temperature results in rapid pyrolysis, often causing cracking and porosity of the developing film. Accurate knowledge of the decomposition temperature is therefore essential to design an appropriate heat treatment, and assuming the 26–64 °C higher temperatures previously reported is likely to result in poor coating morphology.

5. Conclusions

The dehydration and decomposition of $Ba(CF_3COO)_2{\cdot}nH_2O$ have been investigated in flowing dry Ar, and both wet and dry flowing O_2. It has been determined by HR-TG that the salt is a dihydrate ($n = 1.9 \pm 0.1$), with dehydration proceeding in three steps. Decomposition to BaF_2 takes place in two stages, probably via the unstable intermediate $CF_3COOBaF$, by the liberation of CO_2 and the:CF_2 diradical. In the presence of water, the latter forms HF, causing the formation of other fluorinated species; but fluorophosgen (carbonyl difluoride, COF_2) was not detected. The decomposition temperatures, 282–292 °C, were significantly lower than previously reported.

Acknowledgements

Mariusz Mosiadz would like to thank Mr. Robert Cornell (Polymer Characterisation Laboratory, Department of Materials Science and Metallurgy, University of Cambridge) for help with thermal analysis. Katarzyna Juda would like to gratefully acknowledge the Socrates-Erasmus Exchange Programme of the European Commission for financial support. This research was funded by the European Commission 6th Framework Programme (MRTN-CT-2006-035619), Marie Curie Action NESPA project (NanoEngineered Superconductors for Power Applications).

References

[1] M.G. Drexhage, Glass IV, in: M. Tomozawa, R. Doremus (Eds.), Treatise on Material Science and Technology, vol. 26, Academic Press Inc., New York, 1985, p. 151.
[2] M. Poulain, Halide glasses, J. Non-Cryst. Solids 56 (1983) 1–14.
[3] H.K. Pulker, Characterization of optical thin films, Appl. Opt. 18 (1979) 1969–1977.
[4] R. Thielsch, H. Bottcher, Preparation and properties of Ge microcrystals in MgF_2 layers, Chem. Phys. Lett. 189 (1992) 226–230.
[5] T. Furubayashi, I. Nakataki, Superparamagnetism of granular Fe–MgF_2 films, IEEE Trans. Magn. 34 (1998) 1117–1119.
[6] C. Buchal, et al., 1.5 μm photoluminescence of Er^{3+} in YF_3, LuF_3, and LaF_3 thin films, Appl. Phys. Lett. 68 (1996) 438–440.
[7] J. Lau, A.M. Nakata, J.D. Mackenzie, Influence of drawing temperature on the strength of fluoride glass fibers, J. Non-Cryst. Solids 70 (1985) 233–242.
[8] H. Poignant, C. Falcou, J. Le Mellot, The preparation of fluoride glass single mode fibres, Glass Technol. 28 (1987) 38–42.
[9] A. Gupta, R. Jagannathan, E.I. Cooper, E.A. Giess, J.I. Landman, B.W. Hussey, Superconducting oxide films with high transition temperature prepared from metal trifluoroacetate precursors, Appl. Phys. Lett. 52 (1988) 2077–2079.
[10] C. Rüssel, A pyrolytic route to fluoride glasses. I. Preparation and thermal decomposition of metal trifluoroacetates, J. Non-Cryst. Solids 152 (1993) 161–166.
[11] U. Wagener, C. Russel, A pyrolytic route to fluoride glasses. II. Preparation of glasses in the system ZrF_4–BaF_2–LaF_3–$A1F_3$–NaF, J. Non-Cryst. Solids 152 (1993) 167–171.
[12] W. Mahler, The inorganic chemistry of carbon difluoride, Inorg. Chem. 2 (1963) 230.
[13] S. Sathyamurthy, K. Salama, Processing of $YBa_2Cu_3O_x$ films by solution techniques using metal–organic decomposition, J. Supercond. 11 (1998) 545–553.
[14] S.M. Mukhopadhyay, J. Su, V. Chintameneni, Solution-based approaches to fabrication of $YBa_2Cu_3O_{7-\delta}$ (YBCO): precursors of tri-fluoroacetate (TFA) and nanoparticle colloids, J. Electron. Mater. 36 (2007) 1243–1251.
[15] G.R. Heal, Thermogravimetry and derivative thermogravimetry, in: P.J. Haines (Ed.), Principles of Thermal Analysis and Calorimetry, The Royal Society of Chemistry, Cambridge, 2002, pp. 10–54.
[16] D.M. Jollie, P.G. Harrison, An in situ IR study of the thermal decomposition of trifluoroacetic acid, J. Chem. Soc. Perkin Trans. 2 (1997) 1571–1575.
[17] G.A. Kuipers, D.F. Smith, A.H. Nielsen, Infrared spectrum of hydrogen fluoride, J. Chem. Phys. 25 (1965) 275–279.
[18] C.J. Pouchert, The Aldrich Library of FT-IR Spectra Vapor Phase, vol. 3, first ed., Aldrich Chemical Company Inc., 1989.
[19] R.L. Redington, Matrix-isolation spectra of 180-substituted trifluoroacetic acid monomers and vibrational assignments for related CF_3-containing molecules, Spectrochim. Acta A 31 (1975) 1699–1705.
[20] R.E. Kagarise, Infrared spectrum of trifluoroacetic acid vapor, J. Chem. Phys. 27 (1957) 519–522.
[21] M.P. Casassa, D.S. Bomse, K.C. Janda, Infrared photodissociation of van der Waals molecules containing ethylene, J. Chem. Phys. 74 (1981) 5044–5056.
[22] J. Pola, Z. Bastl, J. Tlaskal, Infrared-laser induced production of silicon coating via reaction of silane with trifluoroacetic acid, Infrared Phys. 30 (1990) 355–357.
[23] R.A. Mitsch, Difluorodiazirine. II. Difluoromethane derivatives, J. Heterocycl. Chem. 1 (1964) 223–234.
[24] T. Shimanouchi, Tables of molecular vibrational frequencies. Consolidated volume II, J. Phys. Chem. Ref. Data 6 (1977) 993–1103.
[25] K.W. Rillings, J.E. Roberts, A thermal study of the trifluoroacetates and pentafluoropropionates of praseodymium, samarium and erbium, Thermochim. Acta 10 (1974) 285–298.
[26] P.G. Blake, H. Pritchard, The thermal decomposition of trifluoroacetic acid, J. Chem. Soc. B (1967) 282–286.
[27] J. Pola, Z. Basti, J. Tlaskal, Infrared-laser induced production of silicon coating via reaction of silane with trifluoroacetic acid, Infrared Phys. 30 (1990) 355–357.
[28] J.P. Simons, A.J. Yarwood, Production and properties of di-fluorocarbene, Nature 192 (1961) 943–944.
[29] H.C. Clark, C.J. Willis, Perfluoroalkyl derivatives of tin. I. Trimethyltrifluoromethyltin 1, J. Am. Chem. Soc. 82 (1960) 1888–1891.
[30] M. Tada, S. Fujihara, T. Kimura, Sol–gel processing and characterization of alkaline earth and rare-earth fluoride thin films, J. Mater. Res. 14 (1999) 1610–1616.
[32] C.J. Brinker, G.W. Scherer, Sol–Gel Science: The Physics and Chemistry of Sol–Gel Processing, Academic Press Inc., San Diego, 1990.